



Analysis of the optical properties of ZnO semiconductor nanoparticles obtained using *Artemisia ludoviciana* and their influence on the photocatalytic removal of methyl orange

E. Silva¹ · A. R. Vilchis-Nestor² · A. Castro-Beltran¹ · P. A. Luque³

Received: 11 April 2023 / Accepted: 30 June 2023 / Published online: 15 July 2023

© The Author(s), under exclusive licence to Springer Science+Business Media, LLC, part of Springer Nature 2023

Abstract

This paper reports on a simple and efficient process to obtain semiconductor zinc oxide (ZnO) nanoparticles (NPs) using *Artemisia ludoviciana* extract as a chelating agent. The properties of the ZnO NPs were analyzed using various characterization techniques, revealing hexagonal and quasi-spherical NPs with sizes going from 30.46 to 16.74 nm and band gap values of 2.5 to 2.2 eV. Additionally, the structural analysis shows a wurtzite phase with no secondary phases, while elemental analysis revealed both the presence of residual carbon from *Artemisia ludoviciana* and the presence of oxygen vacancies. The photocatalytic assay of the obtained ZnO showed excellent methyl orange (MO) degradation. The best performance was observed with E4, which removed 95.8% of MO after being exposed to UV light for 120 min. The results demonstrate that the ZnO NPs obtained using *Artemisia ludoviciana* have good photocatalytic capabilities and show potential to be used in other similar applications.

Keywords ZnO · *Artemisia ludoviciana* · Semiconductor · Photocatalysis

1 Introduction

Semiconductors are solid materials whose conductivity and band gap energy fall in the middle of insulators and conductors and have been applied in many fields, going from energy generation (Yang et al. 2017) to environmental remediation (Robertson 1996), biomedical devices (Rotenberg and Tian 2018), and even consumer electronics (Song et al. 2021). Due to their relatively low band gap, the electrical properties of semiconductor materials can be modified through applying external stimuli such as temperature, pressure,

✉ P. A. Luque
pluque@uabc.edu.mx

¹ Facultad de Ingeniería Mochis, Universidad Autónoma de Sinaloa, Los Mochis C.P. 81223, México

² Centro Conjunto de Investigación en Química Sustentable, UAEM-UNAM, Toluca C.P. 50200, México

³ Facultad de Ingeniería, Arquitectura y Diseño, Universidad Autónoma de Baja California, Ensenada C.P. 22860, México

electrical fields or light (Terna et al. 2021). These stimuli induce the promotion of electrons present in the semiconductor's valence band (VB) towards the conduction band (CB), resulting in free electrons and the "holes" they leave behind, which are collectively known as charge carriers (Gomathi and Kumaraguru 2018). These electrons and holes are vital in various photocatalytic reactions such as water-splitting, CO₂ reduction, and oxidation processes (Wang et al. 2018). In this vein, nanostructured semiconductor materials have attracted interest due to their enhanced properties, such as larger surface area, which in turn increases available reactive sites for surface-dependent processes, including photocatalysis (Lee and Jang 2014). ZnO has been considered a cost-effective alternative for photocatalysis (Tan et al. 2022). It is a wide band-gap semiconductor with great chemical stability, high redox potential, favorable optical and electronic properties, high electron mobility, and good photocatalytic activity (Qi et al. 2017). Additionally, its cost is lower than other widely used semiconductors, such as TiO₂ (Sosa Lissarrague et al. 2023). However, ZnO has some drawbacks preventing its widespread use, such as the high recombination rate of the electron-hole pair preventing charge carriers from reaching the surface and limiting the efficiency of the material (Nadeem et al. 2022). Various alternatives have been investigated to resolve these limitations, such as doping (Mirzaeifard et al. 2020), photosensitization (Youssef et al. 2018), the formation of nanocomposites (Sardar et al. 2023), or the introduction of surface defects such as oxygen vacancies (Xu et al. 2020). Furthermore, while ZnO can be obtained through several methods including sol-gel (Perveen et al. 2020), spray pyrolysis, hydrothermal synthesis (Wang et al. 2013), chemical deposition (Tiwari et al. 2022), among others (Hessien 2022), these methods have their own drawbacks, whether it be high production costs, elevated energy demand, or the use of toxic reagents (Madhumitha et al. 2015). In this day and age, as global warming and pollution become increasingly relevant concerns, the development of more environmentally friendly synthesis procedures has become a primary drive of many researchers (Xu et al. 2021). One of the main routes through which we can obtain semiconductor nanoparticles in a more sustainable manner involves the use of microorganisms, fungi, or plant derived substances as reducing or chelating agents. This eliminates the need for toxic chemicals and is often carried out under low temperatures. In addition, this methodology can help in size-control of the final product, as well as produce materials with various morphologies: nanoparticles (Alsmadi et al. 2022), nanorods (El-Maghrabi et al. 2021), and flower-shaped particles (Khan et al. 2014) have all been previously obtained through plant-assisted synthesis, and there are several reports of plant-mediated ZnO NPs used in the photocatalytic removal of dyes. Gawade et al. in 2017 used *Calotrophis procera* in the green synthesis of ZnO and reported 80% degradation after 180 min of exposure to UV light (Gawade et al. 2017). Chen et al. in 2019 used *Scutellaria baicalensis* for the green synthesis of ZnO, which showed good degradation of MB under UV irradiation (Chen et al. 2019). Ahmed et al. used *Hibiscus sabdariffa* in the synthesis of ZnO NPs for RhB degradation and found good results (Alshamsi and Jaffer 2022), Gayathri et al. used extract of Citrus lemon to obtain ZnO NPs with good photocatalytic activity (Gayathri Devi et al. 2023). *Artemisia ludoviciana* (commonly known as "estafiate") is a medicinal plant which has been traditionally used to treat gastrointestinal and pulmonary infections (Gálvez Romero et al. 2022), as well as an antiparasitic (Ezeta-Miranda et al. 2020). This plant has been reported to contain high amounts of organic compounds, mainly terpenes, and flavonoids (Anaya-Eugenio et al. 2014), and as such is suitable for use as a chelating agent in the fabrication of ZnO NPs. The present work provides a simple and efficient process to obtain semiconductor ZnO NPs with great optical and structural properties, as well as the evaluation of their photocatalytic activity, demonstrating good promise for various applications.

2 Experimental

2.1 Preparation of *Artemisia ludoviciana* extract

A simple infusion procedure was followed to obtain the plant extract using locally purchased *Artemisia ludoviciana* leaves and deionized water. To start, differing contents of the *Artemisia ludoviciana* leaves (0.5 g, 1.0 g, and 2.0 g) were placed in 0.05 L of deionized water. Subsequently, the samples were stirred for a 2 h period to ensure proper hydration. Following this, the mixture of water and plant leaves was transferred to a 60 °C bath for 1 h. Finally, the plant leaves were removed through filtering, and the *Artemisia ludoviciana* extract was obtained.

2.2 Synthesis of semiconductor ZnO

The ZnO NPs were synthesized using the previously prepared *Artemisia ludoviciana* extracts. Initially, the obtained extract was added to a beaker, and then 2 g of the zinc precursor ($\text{Zn}(\text{NO}_3)_2 \cdot 6\text{H}_2\text{O}$, 98%, Sigma-Aldrich) was mixed into it. This solution was mixed for 1 h. Afterward, the uncovered solutions evaporated in a 60 °C water bath until a viscous consistency was obtained. The samples were then placed into and oven at 400 °C and heat treated for 1 h. The resulting solid was finally pulverized manually. This procedure was followed for the three variations of extract concentration, labeled E1, E2, and E4 for 0.5 g, 1.0 g, and 2.0 g, respectively.

2.3 Characterization of ZnO NPs

The properties of the obtained ZnO semiconductor materials were studied through various techniques. UV-visible (UV-vis) absorbance data was acquired by a Perkin Elmer Lambda 365 spectrophotometer. Photoluminescence (PL) spectra were obtained by a Horiba Nanolog spectrometer. X-ray photoelectron spectroscopy (XPS) spectra and high-resolution data of the main elements were obtained using an XPS SPECS PHOIBOS 100 analyzer. Fourier transform infrared (FTIR) spectra were obtained through a Perkin Elmer Spectrum Two spectrophotometer. X-ray diffraction (XRD) patterns were acquired on a Bruker D2-Phase Diffractometer. Transmission electron microscopy (TEM) images were acquired on a JEOL JSM-6310LV microscope. Scanning electron microscopy (SEM) images were obtained through a JEOL JSM-6310LV microscope.

2.4 Photocatalytic activity assessment

The photocatalytic performance of the photocatalysts was studied through the degradation of methyl orange dye (90% purity, FagaLab) under UV radiation. First, a 15 ppm solution of MO was prepared. Then, 50 mg of the ZnO photocatalysts were added to 50 mL of MO solution. The catalyst/dye solution was then left stirring in darkness for 30 min. Afterwards, the dye-photocatalyst mixture was exposed to UV radiation for

120 min. Over the course of this period, samples were collected every 20 min, and later analyzed through UV-vis spectroscopy to monitor the concentration.

3 Results and discussion

3.1 Analysis of optical properties

The UV-vis spectra of E1, E2, and E4 is shown in Fig. 1a. The spectra for E1 shows a distinctive absorption peak at 375 nm, which is associated to surface plasmon resonance phenomenon characteristic to ZnO (Vala et al. 2022). This result confirms the formation of ZnO for all samples, while the sharp peaks suggest small nanosized particles with good size distribution (Satheskumar et al. 2020). On the other hand, the PL spectra (Fig. 1b) shows that all three samples exhibit broad emissions in the 380–550 nm region, per what has been reported in the literature (Lam et al. 2014). The peaks in the visible range of the spectrum 422.3 nm, 450.6 nm, 467.8 nm, 481.9 nm, and 492.5 nm are associated to various defect states (Sun et al. 2013). In more detail, the peaks appearing around 422.3 and 450.6 nm can be related to interstitial Zn, the peak at 467.8 nm is related to Zn vacancies, while the emission at 492.5 nm is attributed to transitions involving oxygen vacancies (Mishra et al. 2010).

Furthermore, the absorbance data from UV-vis characterization was used to estimate the band gap energy for all three ZnO samples following Tauc's model (Dolgonos et al. 2016) and the Energy equation (Fatima et al. 2023; Munawar et al. 2020b). The resulting graphs are shown in Fig. 1c–e, the obtained values were 2.5 eV for E1, 2.4 eV for E2, and

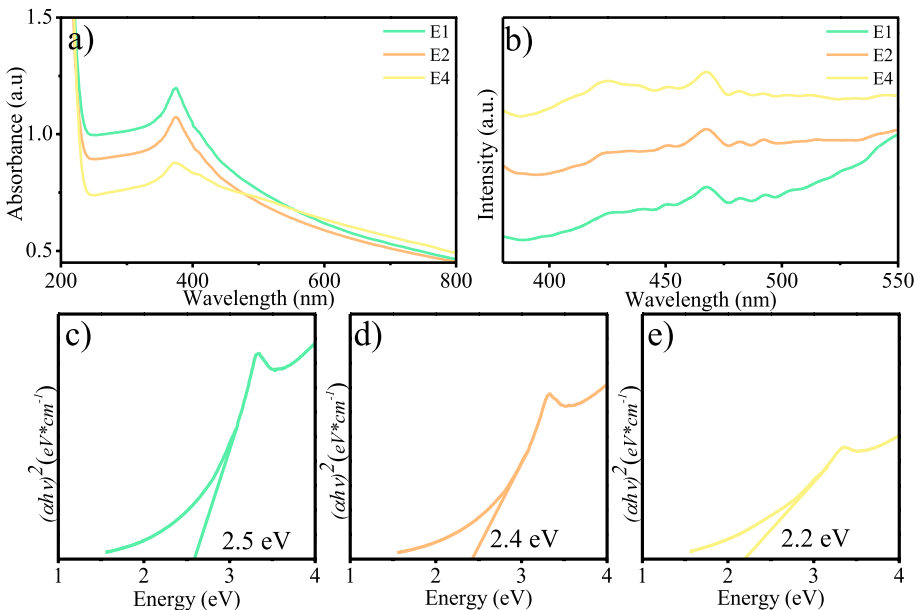


Fig. 1 a UV-vis absorption spectra, b PL emission spectra and c,d,e Tauc plots of the *Artemisia ludoviciana*-mediated ZnO NPs

2.2 eV for E4. Moreover, it was observed that the band gap energy was lower for the NPs synthesized with higher concentrations of *Artemisia ludoviciana*. This can be attributed to the oxygen vacancies, as it has been reported that such defects cause the formation of intermediate energy states, thus producing a decrease in the band gap, which is in agreement with the PL analysis (Li et al. 2022). Additionally, the NPs can show quantum confinement at smaller sizes, which can be responsible for a lower band gap (Babu et al. 2018).

3.2 Morphology and structural analysis

The morphology of the ZnO NPs was studied using transmission electron microscopy. Figure 2 shows TEM images, size distribution, HRTEM, and selected area diffraction patterns of E1, E2, and E4. The TEM (Fig. 2a–c) images of all three ZnO samples show the presence of well-defined nanoparticles with hexagonal to spherical shape and sizes of 30.46 nm for E1 (Fig. 2d), 20.38 nm for E2 (Fig. 2e), and 16.74 nm for E4 (Fig. 2f). We can observe the NPs size diminishes as the concentration of extract goes higher. The change in the NP size is a phenomenon that has been reported previously and is attributed to the organic molecules from *Artemisia ludoviciana* acting as stabilizing and chelating agents, inhibiting, or preventing further growth of the NPs during synthesis (Christensen et al. 2011; Fowsiya et al. 2016).

The high-resolution TEM micrographs (HRTEM) and the selected area diffraction patterns (SAED) were analyzed to examine atomic arrangement and measure the interplanar distance of the NPs. The HRTEM image of E1 (Fig. 2g) shows the presence of several crystallographic planes with an interplanar distance of around 0.253 nm, which can be matched to the main (110) plane in wurtzite phase ZnO (Klinbumrung et al. 2022). Likewise, E2 (Fig. 2h) and E4 (Fig. 2i) measured interplanar distances of 0.255 and 0.250 nm, both of which match the (110) plane of ZnO. Furthermore, the selected area electron diffraction (SAED) pattern for E1 (Fig. 2j) shows a pattern of dots and rings, indicating a crystalline structure. The dots were matched to the (100), (101), (102), and (103) planes of wurtzite ZnO (Vinotha et al. 2019), which is consistent with XRD analysis. For E2 (Fig. 2k) and E4 (Fig. 2l), the SAED patterns show similar well-defined dots and rings, which match the main planes of the ZnO wurtzite structure.

The SEM images and the Energy Dispersive X-Ray analysis (EDX) are shown in Fig. 3. Analysis of the micrographs reveals the formation of large aggregates for all three samples (Kwabena et al. 2019). Similar to TEM results, we can observe a decrease in size for the ZnO NPs obtained using higher concentrations of *Artemisia ludoviciana* extract, confirming the influence of the extract on the properties of synthesized ZnO. Meanwhile, EDX data shows the presence of Zn and O elements, as well as a significant amount of C, due to residual content from the extract's carbon-rich organic molecules (Verbič et al. 2023).

X-ray diffraction was used to analyze the crystalline structure and confirm the phase of the obtained NPs. The diffraction patterns for E1, E2, and E4 are shown in Fig. 4. The same diffraction peaks were observed for the 3 samples. The peak at 31.75° corresponds to (100) plane, the one at 34.42° to (002), 36.25° to (101), 47.54° to (102), 56.60° to (110), 62.87° to (103), and 67.97° to (112). These planes match a hexagonal structure, identifying the obtained material as wurtzite phase ZnO (according to JCPDS no. 36-1451) (Falamas et al. 2022). The diffractograms display no other peaks, thus confirming the ZnO NPs are free of impurities. On the other hand, we can observe a slight broadening and decrease in intensity for the samples obtained using higher concentrations of *Artemisia ludoviciana*. This is reflected in the crystallite size, calculated using Scherrer's formula (Kumar et al.

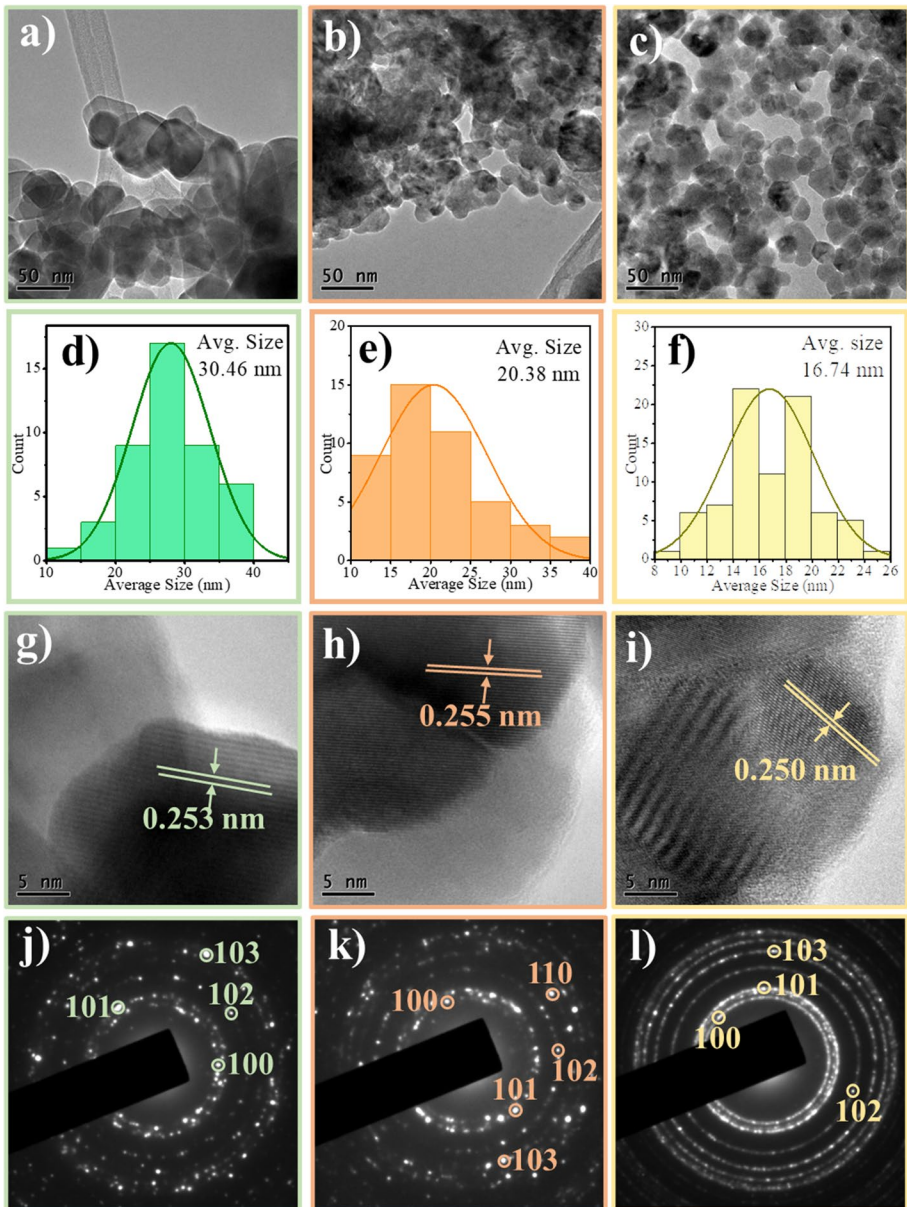


Fig. 2 TEM micrographs, size distribution, HRTEM, and SAED diffraction patterns of *Artemisia ludoviciana*-mediated ZnO NPs: E1 **a,d,g,j**, E2 **b,e,h,k**, and E4 **c,f,i,l**

2019). The obtained values were 35.94 E1 for nm, 23.96 nm for E2, and 11.5 nm for E4. This is similar to the NP size observed in TEM images, and indicates the individual ZnO nanoparticles are comprised mainly by few large crystals (Basak et al. 2022). The XRD data was further analyzed to find the lattice parameters and average d-spacing (Mukhtar et al. 2021a, b, 2022). The results are shown in Table 1.

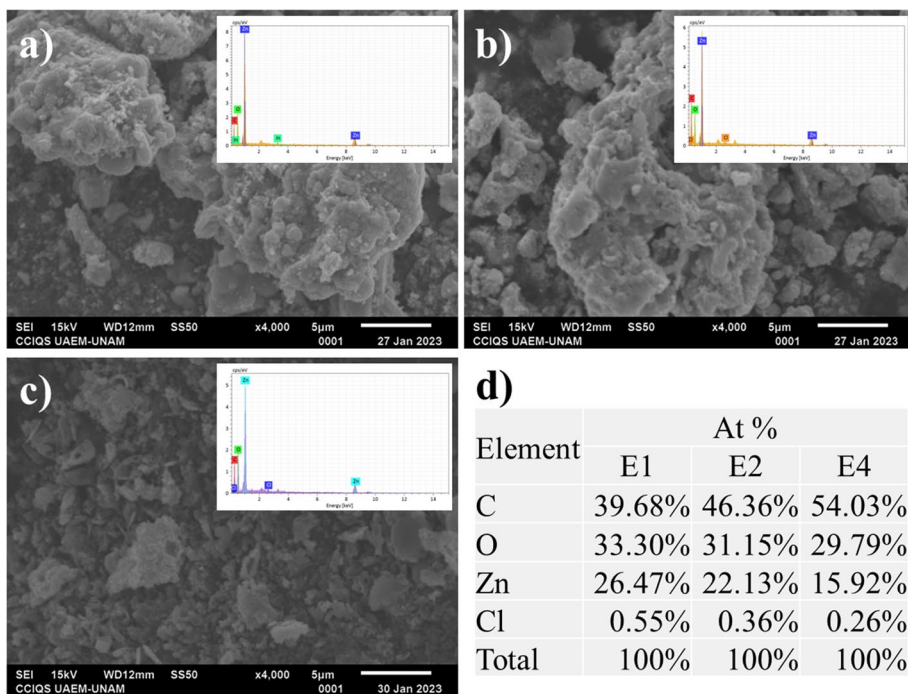


Fig. 3 a-c SEM images and **d** EDX analysis of *Artemisia ludoviciana*-mediated ZnO NPs

3.3 FTIR spectroscopy

The FTIR spectra for *Artemisia ludoviciana* extract and the ZnO NPs (E1, E2, and E4) are displayed in Fig. 5. The FTIR spectrum for *Artemisia ludoviciana* shows a band at 3265 cm^{-1} due to OH bond stretching, as well as a smaller band at 2936 cm^{-1} associated to C–H bond vibrations, while the signals observed at 1407 cm^{-1} and 1358 cm^{-1} are assigned to the bending of O–H bonds in phenolic groups. In addition, the bands at 1615 cm^{-1} and 1724 cm^{-1} are attributed to C=C and C=O bonds present in aromatic rings and carboxyl groups, while the bands at 1015 cm^{-1} and 1055 cm^{-1} correspond to C–O and secondary OH bonds of the polyphenols present in the extract (Owais Mushtaq et al. 2022). In the case of the ZnO NPs, the spectra for E1, E2, and E4 all show the presence of peaks associated to phenolic groups in addition to a band at 400 cm^{-1} , which is associated to stretching vibrational mode of the Zn–O metal-oxygen (Jebali et al. 2023). The presence of both this peak and the characteristic peaks of the main phenolic groups of *Artemisia ludoviciana* extract even after calcination suggests strong interactions with the zinc ions during the synthesis process. These results confirm the functionalization of the extract on the NPs surface and are similar to those previously reported in literature (Yashni et al. 2020).

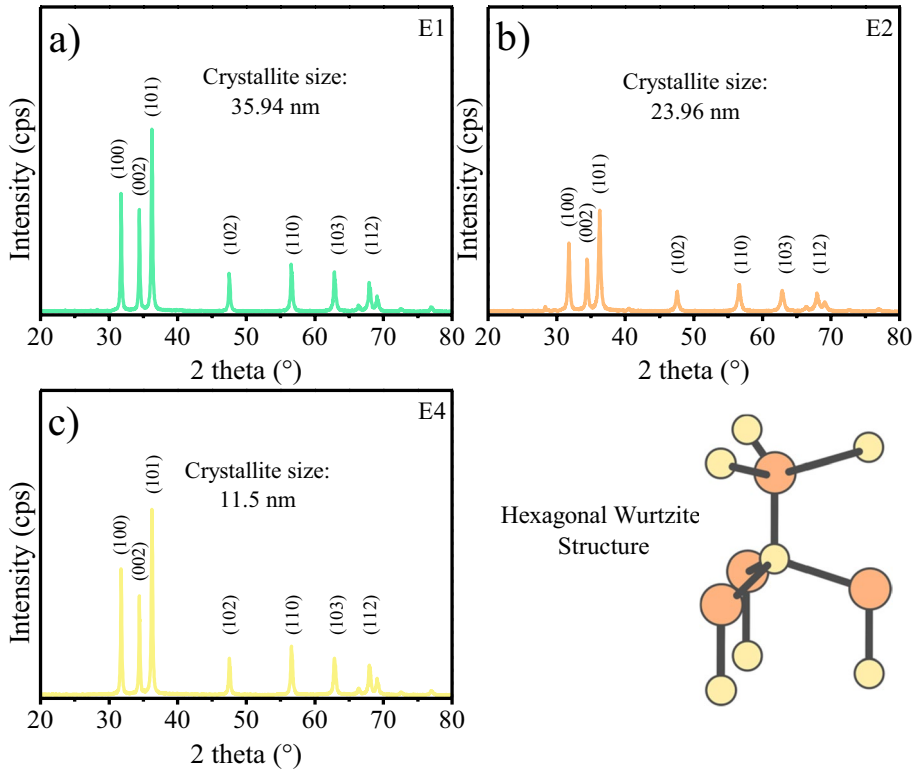


Fig. 4 X-ray diffraction patterns of *Artemisia ludoviciana*-mediated ZnO NPs

Table 1 Lattice parameters of ZnO NPs determined from XRD analysis

Semiconductor	a (Å)	b (Å)	c (Å)	Average d-spacing	Micro-strain ($\times 10^{-3}$)
E1	3.2210	3.2510	5.2070	2.0409	2.61
E2	3.2203	3.2503	5.2027	2.0397	2.82
E4	3.2214	3.2514	5.2063	2.0405	2.88

3.4 X-ray photoelectron spectroscopy (XPS)

Elemental analysis was carried out through XPS spectroscopy. The general wide scan spectra for E1, E2, and E4 are presented in Fig. 6a. The XPS data confirms the presence of Zn and O elements all the obtained ZnO NPs, in addition to C, which indicates the presence of residual carbon from the *Artemisia ludoviciana* extract (Sahai and Goswami 2015). Meanwhile, the Zn2p high-resolution spectra for E1, E2, and E4 is displayed in Fig. 6b. For E1 we can observe two peaks at 1043.7 and 1020.6 eV, which correspond to Zn2p^{1/2} and its doublet at Zn2p^{3/2}, with a difference of 23 eV in binding energy between the two peaks. Likewise, those two peaks also appear in the core-level spectra for E2

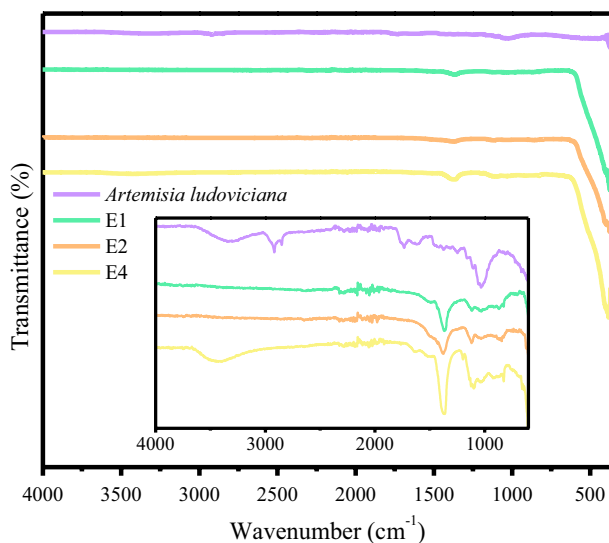


Fig. 5 FTIR spectra of *Artemisia ludoviciana* extract and the *Artemisia ludoviciana*-mediated ZnO NPs

and E4 at similar positions. A single component was found for the three samples, indicating that the oxidation state in all cases was Zn^{2+} (Zhang et al. 2023).

Analysis of the core level O1s peak for E1 (Fig. 6c) reveals the presence of two distinct components. The component that appears at 529.2 eV can be associated to oxygen atoms which form part of the ZnO lattice (Molla et al. 2019), while the other component at 530.8 eV is attributed to surface hydroxyl groups (Joshi et al. 2019). Meanwhile, the high-resolution spectrum of the O1s peak for E2 (Fig. 6d) and E4 (Fig. 6e) both show 3 components. The first one is located at a lower binding energy of 529.6 eV and is assigned to oxygen ions in Zn–O bonding of the ZnO lattice. The next component, positioned at 531.4 eV is associated to oxygen related defects such as vacancies or interstitial atoms (Al-Gaashani et al. 2013), the presence of these vacancies is consistent with the appearance of related peaks in PL spectra (shown in Fig. 1b). Finally, the third peak appearing at 532.4 eV is attributed to the presence of C=O bonds from the *Artemisia ludoviciana* molecules functionalized to the surface (Vilar et al. 2019).

3.5 Evaluation of photocatalytic performance

The photocatalytic performance of the obtained ZnO NPs was studied through the degradation of methyl orange. Figure 7a shows the comparative photocatalytic removal of MO under sunlight for E1, E2, and E4. For all three samples no adsorption was observed during the period of stirring in darkness. The lack of adsorption is attributed to poor interaction between the anionic MO dye molecules and the photocatalyst (Ebrahimian et al. 2020). Once subjected to UV radiation, E1 was able to remove 73.1% of MO after 180 min, while E2 degraded 82.5% in the same time, and E4 showed the best photocatalytic activity with 95.8% of MO removal after only 120 min.

Additionally, degradation rate constants were calculated for all photocatalysts (Fig. 7b). Results showed the reaction kinetics of MB photodegradation followed a pseudo-first order rate for all samples. According to the analysis, approximate k values were 0.00665,

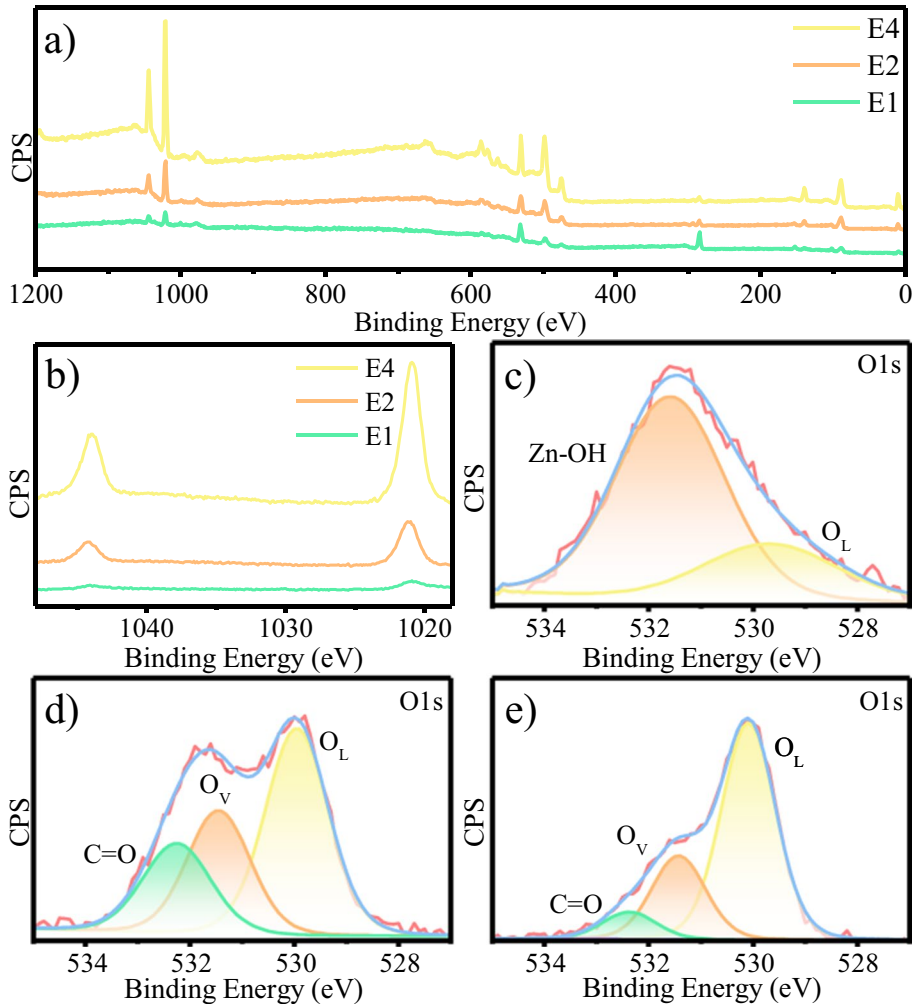


Fig. 6 XPS analysis of *Artemisia ludoviciana*-mediated ZnO NPs: **a** General survey spectra, **b** high resolution spectra for Zn3d peak, and O1s peak deconvolutions for **c** E1, **d** E2, **e** E4

0.00882, and 0.03126 were obtained for E1, E2, and E4, respectively. In general, these values show the effect of the extract concentration during synthesis is an enhancement of the photocatalytic properties for the obtained NPs. This enhanced performance can be attributed to the oxidation of molecules from the extract during synthesis introducing a higher number of oxygen vacancies, generating intermediate energy states to trap electrons and prevent recombination (Acedo-Mendoza et al. 2020), thus increasing photocatalytic efficiency.

The photocatalytic assessment results for ZnO NPs obtained in this study demonstrates their excellent potential for future applications. Table 2 shows a comparison of the photocatalytic degradation of MO using ZnO NPs as reported in the literature.

The mechanism for the photocatalytic degradation of methyl orange is presented in Fig. 8. The photocatalytic process starts with the photo adsorption of radiant energy at the

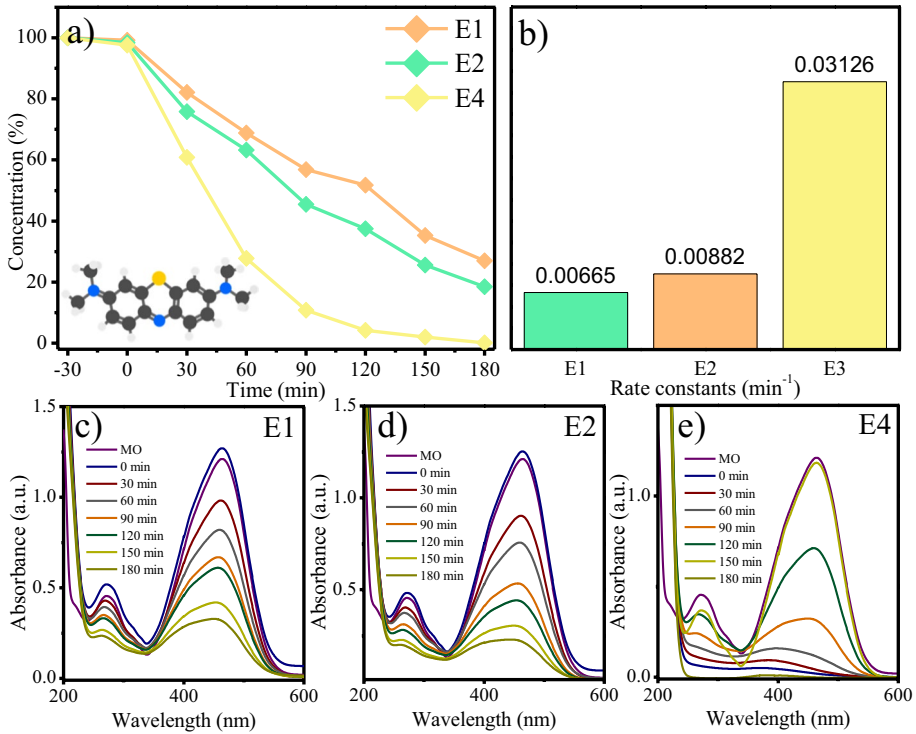


Fig. 7 Photocatalytic degradation of MO under UV irradiation using the *Artemisia ludoviciana*-mediated ZnO NPs: **a** MO concentration over time, **b** degradation rate constants, and absorbance data of MO dye in the presence of **c** E1, **d** E2, and **e** E4

Table 2 Application of different photocatalysts in the degradation of organic dyes

Photocatalyst	Dye	Time (min)	Degradation (%)	Reference
ZnO	MO	80	35	(Chauhan et al. 2020)
ZnO	RhB	120	75	(Rajendrachari et al. 2021)
SnO ₂	RhB	120	46	(Rathinabala et al. 2022)
SnO ₂	MO	180	88	(Gawade et al. 2023)
CuZnCd	MO	50	96.1	(Munawar et al. 2021)
SnO ₂	MO	80	64.3	(Munawar et al. 2022)
SnO ₂ /rGO	MO	80	83.2	
SnZnO ₂ /GO	MO	80	95	
ZnO	MO	120	95.8	This work

surface of a photocatalyst material, like ZnO (Kannan et al. 2022). When a photon with enough energy to breach the bandgap of the material is adsorbed, some of the electrons (e⁻) in the valence band (VB) enter an excited state, moving to the conduction band (CB) and thus generating vacant spaces called “holes” (h⁺) (Alshamsi and Jaffer 2022). Once separated, the e⁻ can convert the O₂ molecules dissolved in the solution into O₂^{*-} radicals

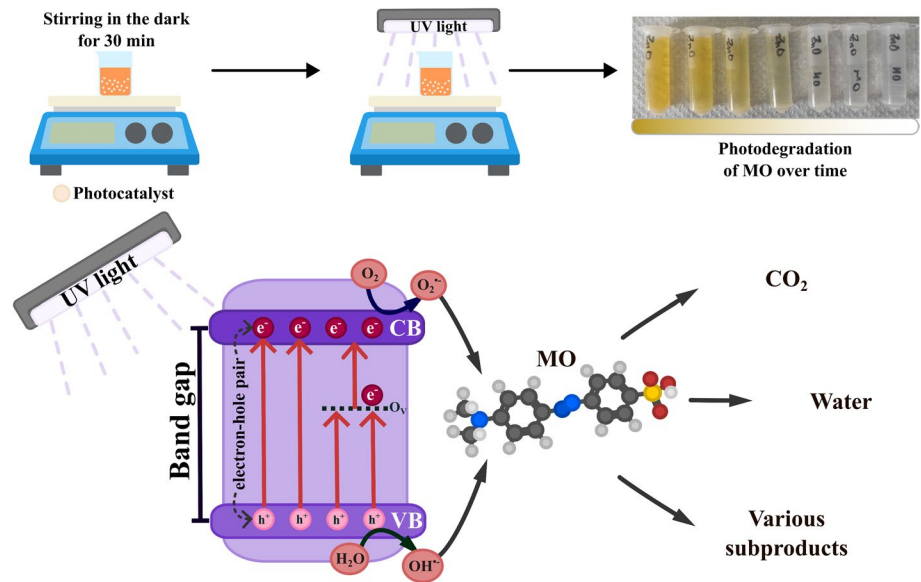


Fig. 8 Schematic of the degradation mechanism of *Artemisia ludoviciana*-mediated ZnO NPs for MO dye degradation under UV light

(Kannan et al. 2020), while the h^+ in the VB of the material can react with the water molecules to produce O_2^* and OH^* species (Mukhtar et al. 2021b; Munawar et al. 2020a). These highly reactive species can then break down the methyl orange molecules into harmless compounds such as H_2O , CO_2 , and other subproducts (Kannan et al. 2021; Nachimuthu et al. 2022).

4 Conclusions

Here we present an efficient and simple method for the fabrication of ZnO NPs with enhanced optical properties. The successful synthesis of ZnO and its functionalization with *Artemisia ludoviciana* extract was confirmed by FTIR and UV-vis characterization. TEM images showed hexagonal NPs with average sizes between 30.46 and 16.74 nm. XRD and SAED patterns indicate the formation of wurtzite phase ZnO with HRTEM confirming a highly crystalline structure. XPS analysis revealed the presence of Zn, O and C elements in the samples, as well as the presence of oxygen defects in the ZnO lattice. Additionally, the photocatalytic assay demonstrated the ZnO NPs excellent potential in the degradation of organic pollutants, with the best sample (E4) being capable of reaching 95.8% degradation of MO in under 120 min of UV light exposure. The high performance of these ZnO NPs demonstrates for the first time that *Artemisia ludoviciana* is a promising source of organic compounds for use in the synthesis of semiconductor NPs with good photocatalytic activity, as well as favorable potential not only for the degradation of different pollutants, but other photocatalytic applications.

Acknowledgements This research was financially supported by CONACYT Grant No. 280518 and Grant A1-S-34533. The authors acknowledgment to Dr. Uvaldo Hernández, M.Sc. Melina Tapia (PXRD) and

B.Sc. María Citlalit Martínez Soto from CCIQS for technical assistance. The authors thank the UABC project number 402/3391.

Author contributions ES: Investigation, Methodology, and Writing - Original Draft. ARV-N: Visualization, Formal Analysis and Writing – Review & Editing. AC-B: Conceptualization, Investigation, and Writing – Review & Editing. PAL: Formal analysis, Supervision, Validation, and Writing – Review & Editing.

Funding This work was supported by by CONACYT Grant No. 280518 and Grant A1-S-34533.

Data availability All data generated or analyzed during this study are included in this published article.

Declarations

Conflict of interest The authors declare no competing interests.

Ethical approval This declaration is not applicable.

References

- Acedo-Mendoza, A.G., Infantes-Molina, A., Vargas-Hernández, D., Chávez-Sánchez, C.A., Rodríguez-Castellón, E., Tánori-Córdova, J.C.: Photodegradation of methylene blue and methyl orange with CuO supported on ZnO photocatalysts: the effect of copper loading and reaction temperature. *Mater. Sci. Semicond. Process* **119**, 105257 (2020). <https://doi.org/10.1016/j.mssp.2020.105257>
- Al-Gaashani, R., Radiman, S., Daud, A.R., Tabet, N., Al-Douri, Y.: XPS and optical studies of different morphologies of ZnO nanostructures prepared by microwave methods. *Ceram. Int* **39**, 2283–2292 (2013). <https://doi.org/10.1016/J.CERAMINT.2012.08.075>
- Alshamsi, H.A., Jaffer, A.A.: New *Hibiscus Sabdariffa* L. petals extract based green synthesis of zinc oxide nanoparticles for photocatalytic degradation of Rhodamine B dye under solar light. In: AIP Conference and Proceedings, p. 2394 (2022). <https://doi.org/10.1063/5.0121228>
- Alsmadi, M.M., Al-Nemrawi, N.K., Obaidat, R., Abu Alkahi, A.E., Korshed, K.M., Lahlouh, I.K.: Nanomedicine Insights into the mapping of green synthesis conditions for ZnO nanoparticles and their toxicokinetics. *Nanomedicine* **17**, 1281–1303 (2022). <https://doi.org/10.2217/NNM-2022-0092>
- Anaya-Eugenio, G.D., Rivero-Cruz, I., Rivera-Chávez, J., Mata, R.: Hypoglycemic properties of some preparations and compounds from Artemisia ludoviciana Nutt. *J. Ethnopharmacol* **155**, 416–425 (2014). <https://doi.org/10.1016/J.JEP.2014.05.051>
- Babu, B., Neelakanta Reddy, I., Yoo, K., Kim, D., Shim, J.: Bandgap tuning and XPS study of SnO₂ quantum dots. *Mater. Lett* **221**, 211–215 (2018). <https://doi.org/10.1016/j.matlet.2018.03.107>
- Basak, M., Rahman, M.L., Ahmed, M.F., Biswas, B., Sharmin, N.: The use of X-ray diffraction peak profile analysis to determine the structural parameters of cobalt ferrite nanoparticles using Debye-Scherrer, Williamson-Hall, Halder-Wagner and size-strain plot: different precipitating agent approach. *J. Alloys Compd.* **895**, 162694 (2022). <https://doi.org/10.1016/J.JALLCOM.2021.162694>
- Chauhan, A., Verma, R., Kumari, S., Sharma, A., Shandilya, P., Li, X., Batoo, K.M., Imran, A., Kulshrestha, S., Kumar, R.: Photocatalytic dye degradation and antimicrobial activities of pure and Ag-doped ZnO using Cannabis sativa leaf extract. *Sci. Rep.* **10**(1), 7881 (2020). <https://doi.org/10.1038/s41598-020-64419-0>
- Chen, L., Batjikh, I., Hurh, J., Han, Y., Huo, Y., Ali, H., Li, J.F., Rupa, E.J., Ahn, J.C., Mathiyalagan, R., Yang, D.C.: Green synthesis of zinc oxide nanoparticles from root extract of *Scutellaria baicalensis* and its photocatalytic degradation activity using methylene blue. *Optik* **84**, 324–329 (2019). <https://doi.org/10.1016/j.ijleo.2019.03.051>
- Christensen, L., Vivekanandhan, S., Misra, M., Kumar Mohanty, A.: Biosynthesis of silver nanoparticles using murraya koenigii (curry leaf): an investigation on the effect of broth concentration in reduction mechanism and particle size. *Adv. Mater. Lett.* **2**, 429–434 (2011). <https://doi.org/10.5185/amlett.2011.4256>
- Dolgonos, A., Mason, T.O., Poepplmeier, K.R.: Direct optical band gap measurement in polycrystalline semiconductors: a critical look at the Tauc method. *J. Solid State Chem.* **240**, 43–48 (2016). <https://doi.org/10.1016/j.jssc.2016.05.010>

- Ebrahimiyan, J., Mohsennia, M., Khayatkashani, M.: Photocatalytic-degradation of organic dye and removal of heavy metal ions using synthesized SnO₂ nanoparticles by Vitex agnus-castus fruit via a green route. *Mater. Lett.* **263**, 127255 (2020). <https://doi.org/10.1016/j.matlet.2019.127255>
- El-Maghrabi, N., El-Borady, O.M., Hosny, M., Fawzy, M.: Catalytic and medical potential of a phyto-functionalized reduced Graphene Oxide–Gold Nanocomposite using Willow-Leaved Knotgrass. *ACS Omega* **6**, 34954–34966 (2021). <https://doi.org/10.1021/acsomega.1c05596>
- Ezeta-Miranda, A., Vera-Montenegro, Y., Avila-Acevedo, J.G., García-Bores, A.M., Estrella-Parra, E.A., Francisco-Marquez, G., Ibarra-Velarde, F.: Efficacy of purified fractions of *Artemisia ludoviciana* Nutt. mexicana and ultrastructural damage to newly excysted juveniles of *Fasciola hepatica* in vitro. *Vet. Parasitol.* **285**, 109184 (2020). <https://doi.org/10.1016/J.VETPAR.2020.109184>
- Falamas, A., Marica, I., Popa, A., Toloman, D., Pruneanu, S., Pogacean, F., Nekkavil, F., Silipas, T.D., Stefan, M.: Size-dependent spectroscopic insight into the steady-state and time-resolved optical properties of ZnO photocatalysts. *Mater. Sci. Semicond. Process* **145**, 106644 (2022). <https://doi.org/10.1016/J.MSSP.2022.106644>
- Fatima, S., Munawar, T., Nadeem, M.S., Mukhtar, F., Khan, S.A., Koc, M., Iqbal, F.: Boosted natural sunlight driven photodegradation of organic dyes using rGO anchored Pr/Cu dual-doped ZnO nanocomposite: characterization and mechanistic insight. *Opt. Mater.* **36**, 113397 (2023). <https://doi.org/10.1016/J.OPTMAT.2022.113397>
- Fowsiya, J., Madhumitha, G., Al-Dhabi, N.A., Arasu, M.V.: Photocatalytic degradation of Congo red using *Carissa edulis* extract capped zinc oxide nanoparticles. *J. Photochem. Photobiol. B Biol.* **162**, 395–401 (2016). <https://doi.org/10.1016/j.jphotobiol.2016.07.011>
- Gálvez Romero, J.L., Parada Sosa, C.M., Burgoa, G.L., Lorenzo Leal, A.C., El Kassis, E.G., Bautista Rodríguez, E., Paredes Juárez, G.A., Hernández, L.R., Bach, H., Juárez, Z.N.: Antimicrobial, cytotoxic, and anti-inflammatory activities of *Artemisia ludoviciana*. *J. Ethnopharmacol.* **293**, 115249 (2022). <https://doi.org/10.1016/J.JEP.2022.115249>
- Gawade, V.V., Gavade, N.L., Shinde, H.M., Babar, S.B., Kadam, A.N., Garadkar, K.M.: Green synthesis of ZnO nanoparticles by using *Calotropis procera* leaves for the photodegradation of methyl orange. *J. Mater. Sci. Mater. Electron.* **28**, 14033–14039 (2017). <https://doi.org/10.1007/s10854-017-7254-2>
- Gawade, V.V., Sabale, S.R., Dhabbe, R.S., Garadkar, K.M.: Environmentally sustainable synthesis of SnO₂ nanostructures for efficient photodegradation of industrial dyes. *J. Mater. Sci. Mater. Electron.* **34**, 1–13 (2023). <https://doi.org/10.1007/S10854-022-09455-4/FIGURES/11>
- Gayathri Devi, K., Clara Dhanemozhi, A., Sathya Priya, L.: Green synthesis of zinc oxide nanoparticles using lemon extract for waste water treatment. *Mater. Today Proc.* (2023). <https://doi.org/10.1016/J.MATPR.2023.03.576>
- Gomathi, E., Kumaraguru, K.: Green Synthesis and Photogenerated Charge Carriers transfer in SnO₂ QDs decorated rGO nanosheets for highly efficient visible light photocatalysis. *J. Inorg. Organomet. Polym. Mater.* **28**, 1664–1670 (2018). <https://doi.org/10.1007/s10904-018-0844-5>
- Hessien, M.: Recent progress in zinc oxide nanomaterials and nanocomposites: from synthesis to applications. *Ceram. Int.* **48**, 22609–22628 (2022). <https://doi.org/10.1016/J.CERAMINT.2022.05.082>
- Jebali, M., Colangelo, G., Gómez-Merino, A.I.: Green synthesis, characterization, and empirical Thermal Conductivity Assessment of ZnO Nanofluids for high-efficiency heat-transfer applications. *Mater. (Basel)* (2023). <https://doi.org/10.3390/MA16041542>
- Joshi, N., da Silva, L.F., Shimizu, F.M., Mastelaro, V.R., M'Peko, J.C., Lin, L., Oliveira, O.N.: UV-assisted chemiresistors made with gold-modified ZnO nanorods to detect ozone gas at room temperature. *Microchim. Acta.* **186**, 418 (2019). <https://doi.org/10.1007/S00604-019-3532-4>
- Kannan, K., Radhika, D., Gnanasangeetha, D., Lakkaboyana, S.K., Sadasivuni, K.K., Gurushankar, K., Hanafiah, M.M.: Photocatalytic and antimicrobial properties of microwave synthesized mixed metal oxide nanocomposite. *Inorg. Chem. Commun.* **125**, 108429 (2021). <https://doi.org/10.1016/J.INOCHE.2020.108429>
- Kannan, K., Radhika, D., Kasai, R.D., Gnanasangeetha, D., Palani, G., Gurushankar, K., Koutavarapu, R., Lee, D.Y., Shim, J.: Facile fabrication of novel ceria-based nanocomposite (CYO-CSO) via co-precipitation: electrochemical, photocatalytic and antibacterial performances. *J. Mol. Struct.* **1256**, 132519 (2022). <https://doi.org/10.1016/J.MOLSTRUC.2022.132519>
- Kannan, K., Radhika, D., Nesaraj, A.S., Kumar Sadasivuni, K., Sivarama Krishna, L.: Facile synthesis of NiO-CYSO nanocomposite for photocatalytic and antibacterial applications. *Inorg. Chem. Commun.* **122**, 108307 (2020). <https://doi.org/10.1016/J.INOCHE.2020.108307>
- Khan, R., Khan, M., Hamedullah, M., Ansari, A., Lohani, M.B., Khan, R., Ahmad, I., Husain, F.M., Khan, W., Alam, M.: Flower-shaped ZnO nanoparticles synthesized by a novel approach at near-room temperatures with antibacterial and antifungal properties. *Int. J. Nanomed.* (2014). <https://doi.org/10.2147/IJN.S47351>

- Klinbumrung, A., Panya, R., Pung-Ngama, A., Nasomjai, P., Saowalakmea, J., Sirirak, R.: Green synthesis of ZnO nanoparticles by pineapple peel extract from various alkali sources. *J. Asian Ceram. Soc.* **10**, 755–765 (2022). <https://doi.org/10.1080/21870764.2022.2127504>
- Kumar, V., Singh, S.K., Sharma, H., Kumar, S., Banerjee, M.K., Vij, A.: Investigation of structural and optical properties of ZnO thin films of different thickness grown by pulsed laser deposition method. *Phys. B Condens. Matter* **552**, 221–226 (2019). <https://doi.org/10.1016/J.PHYSB.2018.10.004>
- Kwabena, D.E., Wee, B.S., Fun, C.S., Kok, K.Y., Assim, Z.B., Aquisman, A.E.: Comparative evaluation of Antibacterial Efficacy of Biological synthesis of ZnO Nanoparticles using Fresh Leaf Extract and Fresh Stem-Bark of Carica papaya. *Nano Biomed. Eng.* **11**, 264–271 (2019). <https://doi.org/10.5101/NBE.V11I3.P264-271>
- Lam, S.M., Sin, J.C., Abdullah, A.Z., Mohamed, A.R.: Transition metal oxide loaded ZnO nanorods: preparation, characterization and their UV-vis photocatalytic activities. *Sep. Purif. Technol* **132**, 378–387 (2014). <https://doi.org/10.1016/J.SEPUR.2014.05.043>
- Lee, J.S., Jang, J.: Hetero-structured semiconductor nanomaterials for photocatalytic applications. Elsevier, London (2014)
- Li, H., Liu, J., Wang, C., Yang, H., Xue, X.: Oxygen vacancies-enriched and porous hierarchical structures of ZnO microspheres with improved photocatalytic performance. *Vacuum* **199**, 110891 (2022). <https://doi.org/10.1016/j.vacuum.2022.110891>
- Madhumitha, G., Elango, G., Roopan, S.M.: Biotechnological aspects of ZnO nanoparticles: overview on synthesis and its applications. *Appl. Microbiol. Biotechnol.* **100**, 571–581 (2015). <https://doi.org/10.1007/S00253-015-7108-X>
- Mirzaeifard, Z., Shariatnia, Z., Jourshabani, M., Rezaei Darvishi, S.M.: ZnO Photocatalyst Revisited: Effective photocatalytic degradation of emerging contaminants using S-Doped ZnO nanoparticles under visible light Radiation. *Ind. Eng. Chem. Res.* **59**, 15894–15911 (2020). https://doi.org/10.1021/ACS.IECR.0C03192/SUPPL_FILE/IEO03192_SI_001.PDF
- Mishra, S.K., Srivastava, R.K., Prakash, S.G., Yadav, R.S., Panday, A.C.: Photoluminescence and photoconductive characteristics of hydrothermally synthesized ZnO nanoparticles. *Opto Electron. Rev.* **18**, 467–473 (2010). <https://doi.org/10.2478/S11772-010-0037-4>
- Molla, M.A.I., Furukawa, M., Tateishi, I., Katsumata, H., Kaneco, S.: Studies of effects of calcination temperature on the crystallinity and optical properties of Ag-doped ZnO nanocomposites. *J. Compos. Sci.* **3**, 18 (2019). <https://doi.org/10.3390/JCS3010018>
- Mukhtar, F., Munawar, T., Nadeem, M.S., Naveed ur Rehman, M., Khan, S.A., Koc, M., Batool, S., Hasan, M., Iqbal, F.: Dual Z-scheme core-shell PANI-CeO₂-Fe₂O₃-NiO heterostructured nanocomposite for dyes remediation under sunlight and bacterial disinfection. *Environ. Res.* **215**, 114140 (2022). <https://doi.org/10.1016/J.ENVRES.2022.114140>
- Mukhtar, F., Munawar, T., Nadeem, M.S., ur Rehman, M.N., Mahmood, K., Batool, S., Hasan, M., ur Rehman, K., Iqbal, F.: Enhancement in carrier separation of ZnO-Ho₂O₃-Sm₂O₃ heterostructured nanocomposite with rGO and PANI supported direct dual Z-scheme for antimicrobial inactivation and sunlight driven photocatalysis. *Adv. Powder Technol.* **32**, 3770–3787 (2021). <https://doi.org/10.1016/J.APT.2021.08.022>. (b)
- Mukhtar, F., Munawar, T., Nadeem, M.S., ur Rehman, M.N., Riaz, M., Iqbal, F.: Dual S-scheme hetero-junction ZnO-V₂O₅-WO₃ nanocomposite with enhanced photocatalytic and antimicrobial activity. *Mater. Chem. Phys.* **263**, 124372 (2021). <https://doi.org/10.1016/J.MATCHEMPHYS.2021.124372>
- Munawar, T., Mukhtar, F., Nadeem, M.S., Riaz, M., Naveed ur Rahman, M., Mahmood, K., Hasan, M., Arshad, M.I., Hussain, F., Hussain, A., Iqbal, F.: Novel photocatalyst and antibacterial agent; direct dual Z-scheme ZnO-CeO₂-Yb₂O₃ heterostructured nanocomposite. *Solid State Sci.* **109**, 106446 (2020). <https://doi.org/10.1016/J.SOLIDSTATESCIENCES.2020a.106446>
- Munawar, T., Nadeem, M.S., Mukhtar, F., Rehman, M.N., ur Riaz, M., Batool, S., Hasan, M., Iqbal, F.: Transition metal-doped SnO₂ and graphene oxide (GO) supported nanocomposites as efficient photocatalysts and antibacterial agents. *Environ. Sci. Pollut. Res.* **29**, 90995–91016 (2022). <https://doi.org/10.1007/S11356-022-22144-3/FIGURES/6>
- Munawar, T., Nadeem, M.S., Rehman, M.N., ur Mukhtar, F., Riaz, M., Iqbal, F.: Sol-gel synthesis of Cu_{0.9}Zn_{0.05}M_{0.05}O (M = cr, Co, cd) nanocrystals for removal of pollutant dyes and bacterial inactivation. *J. Mater. Sci. Mater. Electron.* **32**, 14437–14455 (2021). <https://doi.org/10.1007/S10854-021-06003-4/TABLES/7>
- Munawar, T., Yasmeen, S., Mukhtar, F., Nadeem, M.S., Mahmood, K., Saqib Saif, M., Hasan, M., Ali, A., Hussain, F., Iqbal, F.: Zn_{0.9}Ce_{0.05}M_{0.05}O (M = er, Y, V) nanocrystals: Structural and energy bandgap engineering of ZnO for enhancing photocatalytic and antibacterial activity. *Ceram. Int.* **46**, 14369–14383 (2020). <https://doi.org/10.1016/J.CERAMINT.2020.02.232>. (b)

- Nachimuthu, S., Thangavel, S., Kannan, K., Selvakumar, V., Muthusamy, K., Raza Siddiqui, M., Mohammad Wabaidur, S., Parvathiraja, C.: Lawsonia inermis mediated synthesis of ZnO/Fe₂O₃ nanorods for photocatalysis – biological treatment for the enhanced effluent treatment, antibacterial and antioxidant activities. *Chem. Phys. Lett.* **804**, 139907 (2022). <https://doi.org/10.1016/j.cplett.2022.139907>
- Nadeem, M.S., Munawar, T., Mukhtar, F., Batool, S., Hasan, M., Akbar, U.A., Hakeem, A.S., Iqbal, F.: Energy-levels well-matched direct Z-scheme ZnNiNdO/CdS heterojunction for elimination of diverse pollutants from wastewater and microbial disinfection. *Environ. Sci. Pollut. Res.* **29**, 50317–50334 (2022). <https://doi.org/10.1007/S11356-022-19271-2/FIGURES/11>
- Owais Mushtaq, S., Sharma, R., Agrawal, A., Sharma, A., Kumar, S., Awasthi, K., Yadav, C.S., Awasthi, A.: Green synthesis of ZnO nanoparticles from saffron corm extract and their bactericidal activity. *Mater. Today Proc.* **69**, 74–81 (2022). <https://doi.org/10.1016/J.MATPR.2022.09.613>
- Perveen, R., Shujaat, S., Qureshi, Z., Nawaz, S., Khan, M.I., Iqbal, M.: Green versus sol-gel synthesis of ZnO nanoparticles and antimicrobial activity evaluation against panel of pathogens. *J. Mater. Res. Technol.* **9**, 7817–7827 (2020). <https://doi.org/10.1016/J.JMRT.2020.05.004>
- Qi, K., Cheng, B., Yu, J., Ho, W.: Review on the improvement of the photocatalytic and antibacterial activities of ZnO. *J. Alloys Compd.* **727**, 792–820 (2017). <https://doi.org/10.1016/j.jallcom.2017.08.142>
- Rajendrachari, S., Taslimi, P., Karaoglanli, A.C., Uzun, O., Alp, E., Jayaprakash, G.K.: Photocatalytic degradation of rhodamine B (RhB) dye in waste water and enzymatic inhibition study using cauliflower shaped ZnO nanoparticles synthesized by a novel one-pot green synthesis method. *Arab. J. Chem.* **14**, 103180 (2021). <https://doi.org/10.1016/J.ARABJC.2021.103180>
- Rathinabala, R., Thamizselvi, R., Padmanabhan, D., Alshahateh, S.F., Fatimah, I., Sibhatu, K., Kassegn Weldegebrical, A., Abd Razak, G.I., Sagadevan, S.: Sun light-assisted enhanced photocatalytic activity and cytotoxicity of green synthesized SnO₂ nanoparticles. *Inorg. Chem. Commun.* **143**, 109783 (2022). <https://doi.org/10.1016/J.INOCHE.2022.109783>
- Robertson, P.K.J.: Semiconductor photocatalysis: an environmentally acceptable alternative production technique and effluent treatment process. *J. Clean. Prod.* **4**, 203–212 (1996). [https://doi.org/10.1016/S0959-6526\(96\)00044-3](https://doi.org/10.1016/S0959-6526(96)00044-3)
- Rotenberg, M.Y., Tian, B.: Talking to cells: Semiconductor Nanomaterials at the Cellular Interface. *Adv. Biosyst.* **2**, 1700242 (2018). <https://doi.org/10.1002/adbi.201700242>
- Sahai, A., Goswami, N.: Structural and optical investigations of oxygen defects in zinc oxide nanoparticles. *AIP Conf. Proc.* **1665**, 050023 (2015). <https://doi.org/10.1063/1.4917664>
- Sardar, S., Munawar, T., Mukhtar, F., Nadeem, M.S., Khan, S.A., Koc, M., Manzoor, S., Ashiq, M.N., Iqbal, F.: Fullerene triggered energy storage and photocatalytic ability of La₂O₃-ZnO@C60 core-shell nanocomposite. *Mater. Sci. Eng. B* **288**, 116151 (2023). <https://doi.org/10.1016/J.MSEB.2022.116151>
- Satheskumar, M., Anand, B., Muthuvel, A., Rajarajan, M., Mohana, V., Sundaramanickam, A.: Enhanced photocatalytic dye degradation and antibacterial activity of biosynthesized ZnO-NPs using curry leaves extract with coconut water. *Nanotechnol. Environ. Eng.* **5**, 29 (2020). <https://doi.org/10.1007/s41204-020-00093-x>
- Song, C., Yin, C., Qu, H.: Electronic microstructure and thermal conductivity modeling of semiconductor nanomaterials. *Microelectron. J* **108**, 104988 (2021). <https://doi.org/10.1016/j.mejo.2020.104988>
- Sosa Lissarrague, M.H., Alshehri, S., Alsalmi, A., Lassalle, V.L., López Corral, I.: Heavy Metal Removal from Aqueous Effluents by TiO₂ and ZnO Nanomaterials. *Adsorpt. Sci. Technol.* (2023). <https://doi.org/10.1155/2023/2728305>
- Sun, W.J., Li, J., Mele, G., Zhang, Z.Q., Zhang, F.X.: Enhanced photocatalytic degradation of rhodamine B by surface modification of ZnO with copper (II) porphyrin under both UV–vis and visible light irradiation. *J. Mol. Catal. A Chem.* **366**, 84–91 (2013). <https://doi.org/10.1016/J.MOLCATA.2012.09.010>
- Tan, K.W., Yap, C.M., Zheng, Z., Haw, C.Y., Khiew, P.S., Chiu, W.S.: State-of-the-art advances, Development, and Challenges of Metal Oxide Semiconductor Nanomaterials for Photothermal Solar Steam Generation. *Adv. Sustain. Syst.* **6**, 2100416 (2022). <https://doi.org/10.1002/adsu.202100416>
- Terna, A.D., Elemike, E.E., Mbonu, J.I., Osafire, O.E., Ezeani, R.O.: The future of semiconductors nanoparticles: Synthesis, properties and applications. *Mater. Sci. Eng. B* **272**, 115363 (2021). <https://doi.org/10.1016/j.mseb.2021.115363>
- Tiwari, C., Pandey, A., Dixit, A.: Precursor mediated and defect engineered ZnO nanostructures using thermal chemical vapor deposition for green light emission. *Thin Solid Films* **762**, 139539 (2022). <https://doi.org/10.1016/j.tsf.2022.139539>
- Vala, M., Siddhpura, P., Solanki, P., Kataria, B.: Phyllanthus emblica fruit extract assisted green synthesis of ZnO nanoparticles: Thermal, vibrational, optical and electrical properties. *Mater. Today Proc.* **76**, 579–584 (2022). <https://doi.org/10.1016/J.MATPR.2022.11.167>

- Verbič, A., Brenčič, K., Primc, G., Mozetič, M., Šala, M., Gorjanc, M.: Plasma-assisted green synthesis of ZnO directly on Polyethylene Terephthalate Fabric. *Fibers Polym* **24**, 83–94 (2023). <https://doi.org/10.1007/S12221-023-00059-1/FIGURES/8>
- Vilar, V.J.P., Pillai, S.C., Malato, S.: Solar chemistry and photocatalysis: environmental applications. *Environ. Sci. Pollut. Res.* **26**, 36077–6079 (2019). <https://doi.org/10.1007/s11356-019-07334-w>
- Vinotha, V., Iswarya, A., Thaya, R., Govindarajan, M., Alharbi, N.S., Kadaikunnan, S., Khaled, J.M., Al-Anbr, M.N., Vaseeharan, B.: Synthesis of ZnO nanoparticles using insulin-rich leaf extract: Anti-diabetic, antibiofilm and anti-oxidant properties. *J. Photochem. Photobiol B Biol.* **197**, 111541 (2019). <https://doi.org/10.1016/J.JPHOTOBIO.2019.111541>
- Wang, F., Qin, X., Guo, Z., Meng, Y., Yang, L., Ming, Y.: Hydrothermal synthesis of dumbbell-shaped ZnO microstructures. *Ceram. Int* **39**, 8969–8973 (2013). <https://doi.org/10.1016/j.ceramint.2013.04.096>
- Wang, L., Zhao, J., Liu, H., Huang, J.: Design, modification and application of semiconductor photocatalysts. *J. Taiwan. Inst. Chem. Eng* **93**, 590–602 (2018). <https://doi.org/10.1016/j.jtice.2018.09.004>
- Xu, J., Huang, Y., Zhu, S., Abbes, N., Jing, X., Zhang, L.: A review of the green synthesis of ZnO nanoparticles using plant extracts and their prospects for application in antibacterial textiles. *J. Eng. Fiber Fabr.* **16**, 155892502110462 (2021). <https://doi.org/10.1177/15589250211046242>
- Xu, Y., Li, H., Sun, B., Qiao, P., Ren, L., Tian, G., Jiang, B., Pan, K., Zhou, W.: Surface oxygen vacancy defect-promoted electron-hole separation for porous defective ZnO hexagonal plates and enhanced solar-driven photocatalytic performance. *Chem. Eng. J* **379**, 122295 (2020). <https://doi.org/10.1016/J.CEJ.2019.122295>
- Yang, L., Huang, J., Shi, L., Cao, L., Zhou, W., Chang, K., Meng, X., Liu, G., Jie, Y., Ye, J.: Efficient hydrogen evolution over Sb doped SnO₂ photocatalyst sensitized by eosin Y under visible light irradiation. *Nano Energy* **36**, 331–340 (2017). <https://doi.org/10.1016/j.nanoen.2017.04.039>
- Yashni, G., Al-Gheethi, A., Mohamed, R., Shanmugan, V.A., Al-Sahari, M.N.A.: Phytotoxicity evaluation of ZnO nanoparticles synthesized from Coriandrum sativum leaf extract. *Mater. Today Proc.* **47**, 1336–1340 (2020). <https://doi.org/10.1016/J.MATPR.2021.02.816>
- Youssef, Z., Colombeau, L., Yesmurzayeva, N., Baros, F., Vanderesse, R., Hamieh, T., Toufaily, J., Frochot, C., Roques-Carnes, T.: Dye-sensitized nanoparticles for heterogeneous photocatalysis: cases studies with TiO₂, ZnO, fullerene and graphene for water purification. *Dye. Pigment.* **159**, 49–71 (2018). <https://doi.org/10.1016/j.dyepig.2018.06.002>
- Zhang, M., Lin, X., Yi, Z., Xu, X., Yang, J., Zhu, M.: Enhanced reactive oxidation species generation by ligand-to-metal-charge transfer between oxygen vacancy-rich ZnO mesocrystal with ciprofloxacin pollutants. *Appl. Catal. B Environ.* **321**, 122033 (2023). <https://doi.org/10.1016/J.APCATB.2022.122033>

Publisher's Note Springer Nature remains neutral with regard to jurisdictional claims in published maps and institutional affiliations.

Springer Nature or its licensor (e.g. a society or other partner) holds exclusive rights to this article under a publishing agreement with the author(s) or other rightsholder(s); author self-archiving of the accepted manuscript version of this article is solely governed by the terms of such publishing agreement and applicable law.